The CAD Analyses of a Torospheric Head Cover of a Pressurized Cylindrical Fuel Tank after the Crash Test

Prof. PhD. Eng. **Daniela VINTILĂ**[1], Assoc. Prof. PhD. Eng. **Mihai ŢĂLU**[2,*],
Assoc. Prof. PhD. Eng. **Ștefan ŢĂLU**[3]

[1] University of Craiova, Faculty of Mechanics, Department of Applied Mechanics and Civil Engineering, Calea București Street, no. 107, 200512 Craiova, Dolj county, Romania. E-mail: vintila_dnl@yahoo.com

[2] University of Craiova, Faculty of Mechanics, Department of Applied Mechanics and Civil Engineering, Calea București Street, no. 107, 200512 Craiova, Dolj county, Romania. Corresponding author* e-mail: mihai_talu@yahoo.com

[3] Technical University of Cluj-Napoca, The Directorate of Research, Development and Innovation Management (DMCDI), Constantin Daicoviciu Street, no. 15, Cluj-Napoca, 400020, Cluj county, Romania. E-mail: stefan_ta@yahoo.com

§: All authors contributed equally to this work.

Abstract: *The purpose of the study described in this paper was to assess the effect of impact during the crash test on the Von Mises effort state that appear in the end cover on a pressurized cylindrical fuel tank. An optimal CAD design of the torospheric head cover was first determined. The state of stress was determined by the thermal stress and computed by polynomial interpolation. The effectiveness of the method is evaluated by Von Mises stress variance laws during the impact were assessed as well as the influence of the corrosion phenomenon on the state of effort. The obtained results can be applied to experimental modeling of vehicle collision phenomena.*

Keywords: *Automotive industry, corrosion, crash test, industrial engineering design, optimization, pressurized fuel tank, state of effort, torospheric head cover*

1. Introduction

The automotive fuel tank market dynamics offers a vision on the automotive industry trends and help plan effective business strategies based on a rigorous research and analysis of the key data especially over the medium to long term [1-4].
Automotive fuel tank is an important safety and functional part of vehicle used to store liquefied petroleum gas (LPG) or compressed natural gas (CNG) fuel with a complex geometry, made especially of steel or aluminum [5-11].
In computer aided engineering of the fuel tanks structure for representing geometry and material details, various shape design variables [12, 13], structural design variables [14] and software tools [15-20] are used to find an optimal geometrical solution [21-27] at less cost [28-33].
When is installed a pressurized fuel tank for LPG or CNG on a car, it is planned by the automotive constructor to be placed in a special location reinforced and padded with materials capable of amortizing impact shocks resulting from a road accident [5].
The crash test, due to the higher mathematical complexity of a crash event representation, is a special stress test performed on pressurized tanks during the homologation process in which a metal bar is projected in the tank at a speed of v = 15 m/s [31-34].
The selected collision phenomenon is provided by a set of complicated experiments on the sidewalls of the pressurized fuel tank and in particular on the lateral cover or the head cover in case of a cylindrical fuel tank.
In order to generate new dataset which will be used to evaluate the proposed crash modeling methodology, it was decided to create a virtual crash test by numerical simulations to reproduce the test conditions in a realistic manner to be as close as possible to the actual conditions encountered in service. On the other hand, the obtained models and mathematical algorithms are valid only for one given set of collision conditions and increase the cost and time of such simulation [34-37].

There have been numerous examples of applications of fractal and multifractal theory to find patterns in large and complex datasets as in crash data to identify high-crash locations and in traffic management strategies, such as crash analysis, spatial distribution of road traffic accidents and travel time reliability [38-41].

2. The optimal design of the torospheric head cover of the pressurized fuel tank

The torospheric head cover of pressurized fuel tank is calculated by a series of dimensional constructive relations according to the recommendations given by DIN 28011 (Figures 1 and 2).

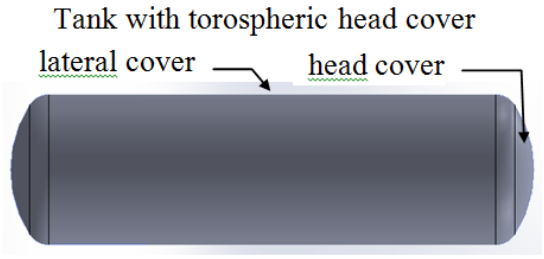

Fig. 1. The components of pressurized fuel tank

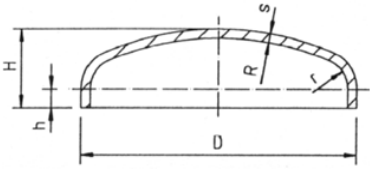

- $r = 0.1 \cdot D$
- $R = D$
- $h \cong 3.5s$
- $H = 0.192D + s + h$

Fig. 2. The sketch of the torospheric lateral cover

2.1. The CAD design of optimal sizing of the head cover

The parameterized modeling of the torospheric head cover (as shown in Figures 3 and 4) was done in the AutoCAD Autodesk 2017 software [42], which was imported to SolidWorks 2017 software [43] for analysis with the: Static, Thermal and Design Study modules.

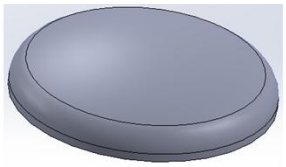

Fig. 3. The model of torospheric head cover

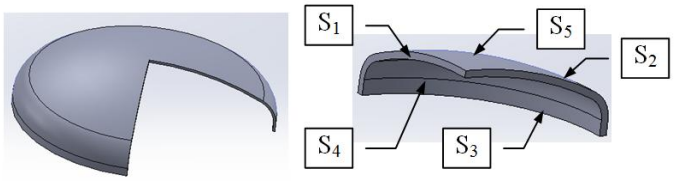

Fig. 4. The ¾ and ¼ sections of torospheric head cover model with indications of the exterior surfaces

The optimization parameters are: thickness s and height h of the torospheric head cover, which have a continuous variation between the limits: s = 2.5...6 mm and h = 10...16 mm.
To evaluate the objective and constraint functions next conditions were imposed:

- obtaining of a maximum resultant Von Mises stress equal to or less than the admissible stress of material AISI 4340, $\sigma_{rez} \leq \sigma_a = 710$ N/mm^2;
- to respect the minimum cover mass condition.

For CAD analysis of the head cover constructive shape a quarter of the model was chosen (due to the model symmetry), (as shown in Figure 4).
The design data used for optimized sizing of cover are:

- non-penetrative torospheric cover with diameter D = 250 mm;
- construction material of the sheet metal: steel AISI 4340;
- geometrical symmetry of S_1 and S_2 surfaces and zero axial displacement of the cover;
- Loads:
  - with maximum pressure of p_{max} = 30 bar on surface S_4;
  - with thermal load between the limits T = -30 ^{0}C up to T = 60 ^{0}C on the surfaces: S_4 and S_5;
  - with a normal impact on the surface S_5 produced with a bar having an initial velocity of v = 15 m /s while impacting the obstacle;
- the duration of the cover exploitation is: n_a = 15 years;
- the corrosion rate of the material is equal to: v_c = 0.06 mm / year.

The optimal values obtained by computation are: s_{opt} = 2.8 mm, and height h = 10 mm. In the same time, the Von Mises maximum stress response occurs at a temperature of T = -30 ^{0}C.

The optimized thickness has been corrected taking into account next factors: the corrosion phenomenon, the negative tolerance of the sheet metal and the thinning phenomenon (by 10 % of the thickness of the laminate to the embossing process).
The formula for calculating the thickness is the following:

$$s_{real} = s_{opt} + v_c \cdot n_a + abs(A_i) + \Delta s_a \quad (1)$$

where:
- v_c, corrosion rate of the cover, v_c = 0.06 mm / year;
- n_a, number of years of exploitation, n_a = 15 years;
- A_i, the lower deviation of the laminate sheet, A_i = - 0.6 mm, for s = 3…5 mm;
- Δs_a = 0.1 s = 0.5 mm, thinning of the sheet caused by the head cover embossing.

Finally, the minimum thickness of the sheet laminate is determined as:

$$s_{real\ min} = 2.8 + 0.06 \cdot 15 + abs(-0.6) + 0.1 \cdot 5 = 4.8 \text{ mm} \quad (2)$$

A laminate sheet of AISI 4340 steel with a thickness of $s = 5^{+0.25}_{-0.6}$ mm is chosen for analysis.
The calculation at impact through numerical simulation was made for n_a = 15 years which corresponds to the end of exploitation time, when the thickness of the head cover is minimal s = 3 mm as a result of corrosion and the Von Mises stress become maximal.

3. The CAD analysis of Von Mises stress in the head cover at the crash test

The impact simulation was considered as a non-linear contact problem. In order to have a basis of comparison at the time of the initial impact, the state of stress due to pressure loading and thermal load was calculated.
Table 1 shows the numerical results of the Von Mises stress as a function of time (for the same interval of time Δt = 5μs and the same interval of temperature at ΔT = 10 ^{0}C). The total impact time was chosen at t = 40 μs.

Table 1: The Von Mises stress during the impact of torospheric head cover

	Temperature T [^{0}C]									
	-30 ^{0}C	-20 ^{0}C	-10 ^{0}C	0 ^{0}C	10 ^{0}C	20 ^{0}C	30 ^{0}C	40 ^{0}C	50 ^{0}C	60 ^{0}C
t [μs]	**Effort state at the time of the initial impact test, σ_i [N/mm^2]**									
0	428.750	426.48	424.31	422.24	420.27	418.4	416.84	416.63	417.71	418.85
5	431.773	429.504	427.335	425.266	423.297	421.428	419.869	419.66	420.743	421.886
10	443.321	441.052	438.883	436.745	434.848	432.981	431.425	431.218	432.30	433.451
15	467.049	464.781	462.614	460.302	458.579	456.712	455.154	454.947	456.029	457.172
20	530.741	537.488	535.335	531.688	531.329	529.475	527.932	527.738	528.834	529.989
25	618.060	615.835	613.709	607.534	609.755	607.927	606.409	606.240	607.360	608.540
30	638.855	636.643	634.531	627.050	630.603	628.789	627.283	627.127	628.260	629.452
35	638.820	636.609	634.496	627.026	630.568	628.753	627.247	627.091	628.224	629.416
	Effort state after t = 40 [μs] from the impact initiation, σ_i [N/mm^2]									
40	638.786	636.574	634.461	627.001	630.533	628.718	627.212	627.055	628.187	629.379

The parameterized model consisting of the head cover and the impact metal bar (with a square section having the side B = 40 mm and the length L = 250 mm), as shown in Figures 5 to 7.

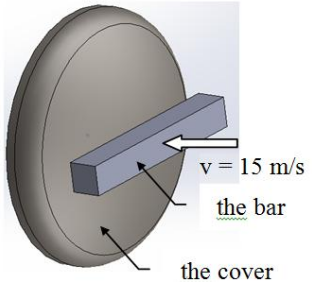

Fig. 5. The isometric view of impact model

Fig. 6. The left view of impact model

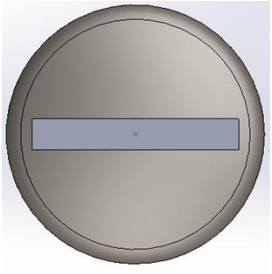

Fig. 7. The front view of impact model

The impact study is carried out in the most unfavorable situation, with the normal incidence of the bar applied on the outer surface of the head cover. At the same time, the bar is in translation along the symmetry axis of the head cover.
Starting from the data in Table 1, the Von Mises maximum stress variation graphs were computed throughout the impact of t = 40 μs for the temperature in range of limits T = -30 ^{0}C up to T = 60 ^{0}C. The laws of variation of stress obtained by polynomial interpolation are represented for each graph (as shown in Figures 7 to 17).

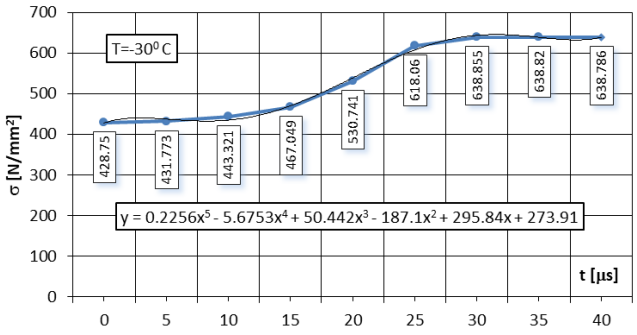

Fig. 8. The Von Mises stress at impact for T = -30 ^{0}C

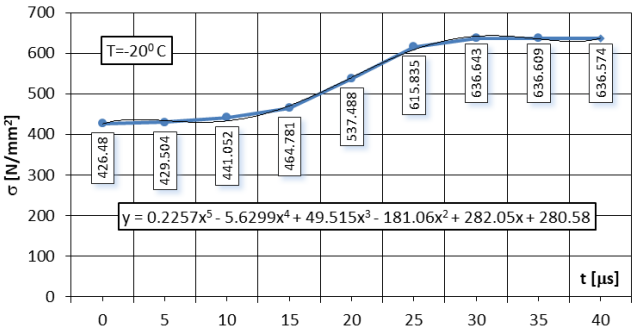

Fig. 9. The Von Mises stress at impact for T = -20 ^{0}C

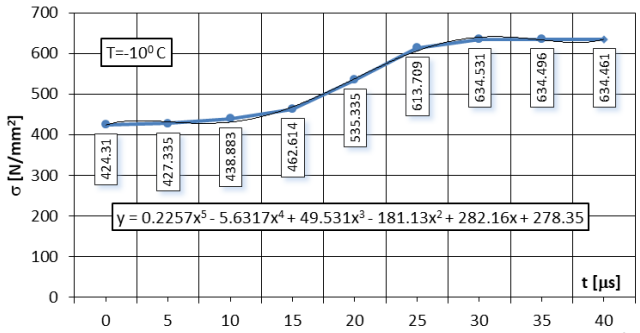

Fig. 10. The Von Mises stress at impact for T = -10 ^{0}C

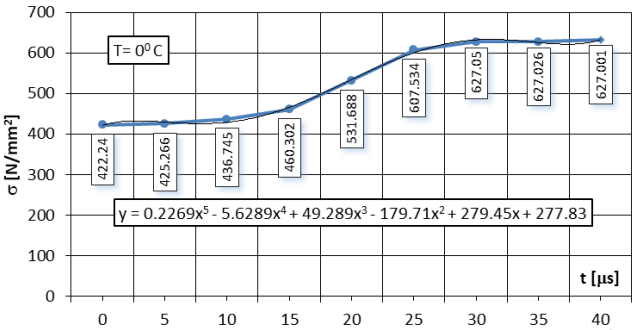

Fig. 11. The Von Mises stress at impact for T = 0 ^{0}C

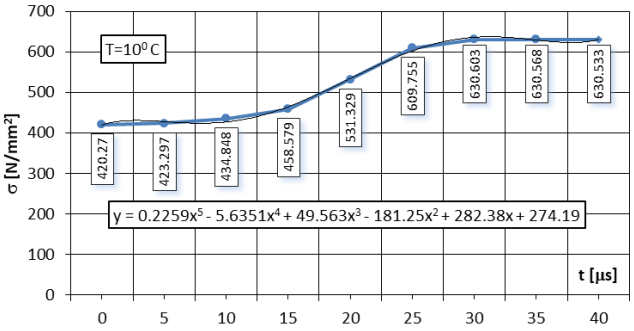

Fig. 12. The Von Mises stress at impact for T = 10 ^{0}C

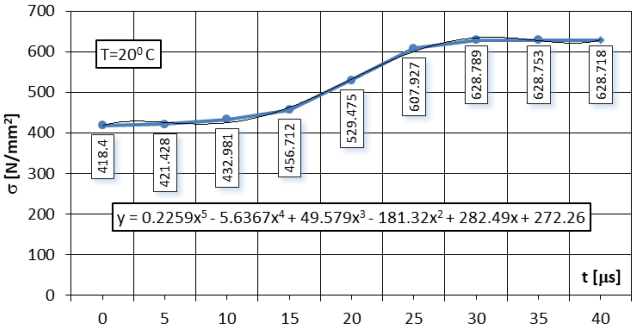

Fig. 13. The Von Mises stress at impact for T = 20 ^{0}C

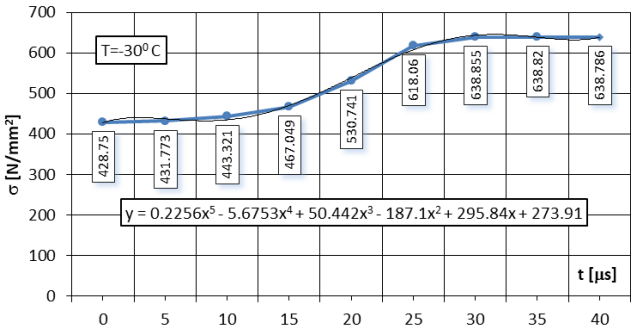

Fig. 14. The Von Mises stress at impact for T = 30 ^{0}C

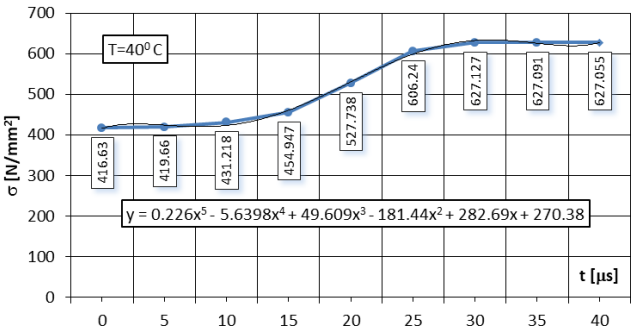

Fig. 15. The Von Mises stress at impact for T = 40 ^{0}C

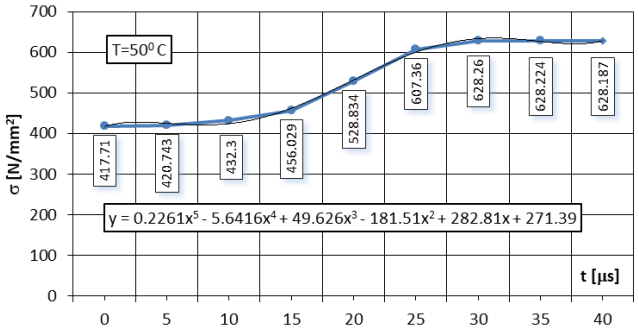

Fig. 16. The Von Mises stress at impact for T = 50 ^{0}C

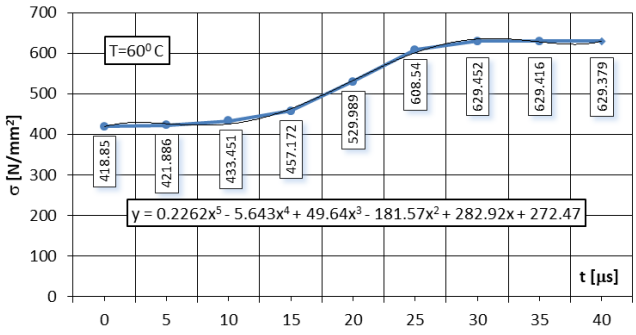

Fig. 17. The Von Mises stress at impact for T = 60 ^{0}C

Graphical representation in axonometric projection of the 3D variation of Von Mises stress state $\sigma(t,T)$ as a result of the cumulative impact-temperature effect produced on the study interval of t = 40 μs is shown in Figure 18. Figure 19 shows a graphical representation of the dependency graph for surface $\sigma(t,T)$ in the top view representation.

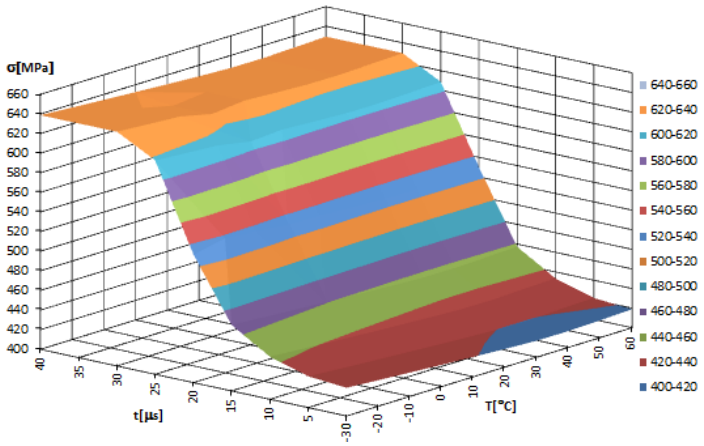

Fig. 18. The graph of Von Mises stress σ(t,T) in torospheric cover

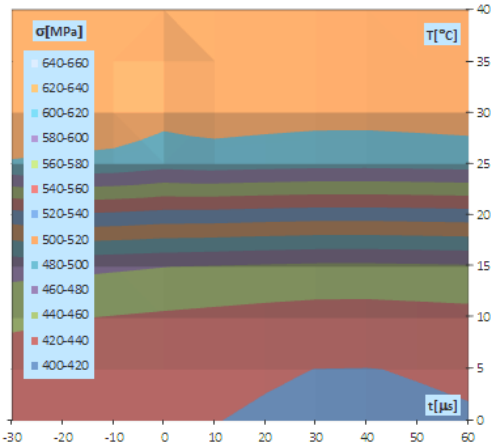

Fig. 19. The superior view of σ(t,T) on the torospheric cover

The variance of Von Mises stress generated only by the impact action, based on the numerical values given in Table 2, was computed and represented in axonometric projection in Figure 20. Figure 21 shows a graphical representation of the dependency graph $\sigma(t,T)$ in the upper view.

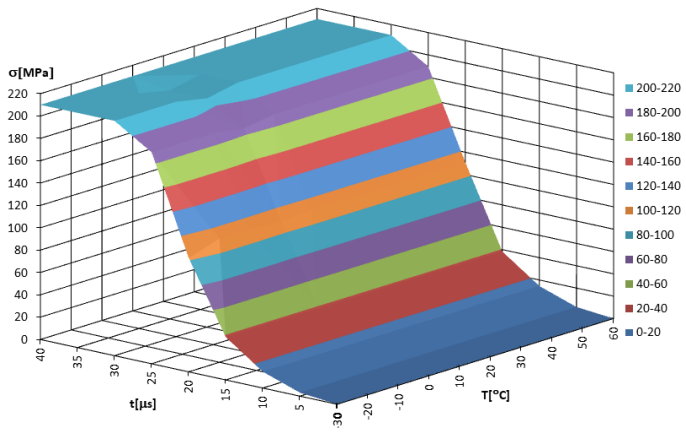

Fig. 20. The graph of Von Mises stress given by the impact in torospheric head cover

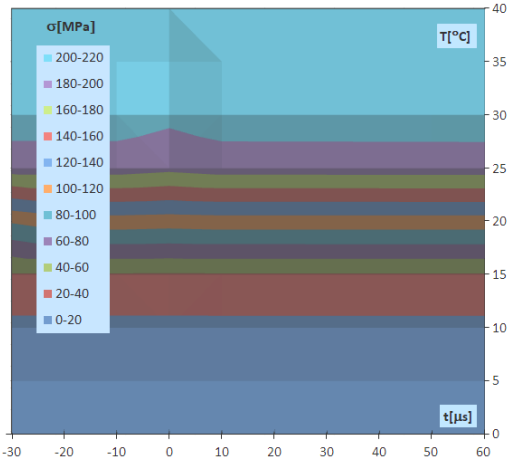

Fig. 21. The superior view of σ(t,T) given by impact on the torospheric head cover

Table 2: The Von Mises stress given only by impact in torospheric head cover

	Temperature T [^{0}C]									
	-30 ^{0}C	-20 ^{0}C	-10 ^{0}C	0 ^{0}C	10 ^{0}C	20 ^{0}C	30 ^{0}C	40 ^{0}C	50 ^{0}C	60 ^{0}C
T[μs]	**Effort state at the time of the initial impact test, σ_i [N/mm^2]**									
0	0	0	0	0	0	0	0	0	0	0
5	3.023	3.024	3.025	3.026	3.027	3.028	3.029	3.03	3.033	3.036
10	14.571	14.572	14.573	14.505	14.578	14.581	14.585	14.588	14.59	14.601
15	38.299	38.301	38.304	38.062	38.309	38.312	38.314	38.317	38.319	38.322
20	101.991	111.008	111.025	109.448	111.059	111.075	111.092	111.108	111.124	111.139
25	189.310	189.355	189.399	185.294	189.485	189.527	189.569	189.61	189.65	189.69
30	210.105	210.163	210.221	204.81	210.333	210.389	210.443	210.497	210.55	210.602
35	210.070	210.129	210.186	204.786	210.298	210.353	210.407	210.461	210.514	210.566
	Effort state after t= 40 [μs] from the impact initiation, σ_i [N/mm^2]									
40	210.036	210.094	210.151	204.761	210.263	210.318	210.372	210.425	210.477	210.529

The envelope stress state computed before the initial impact moment due to variation in temperature and the maximum load pressure on the interior surfaces of toroidal head cover is shown in Figures 22 to 27.

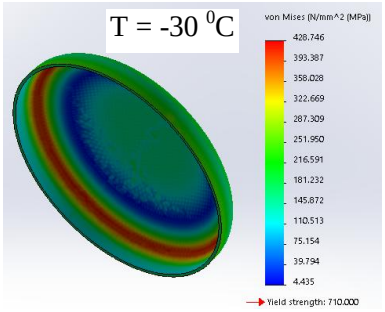

Fig. 22. The Von Mises stress before impact at T = -30 ^{0}C

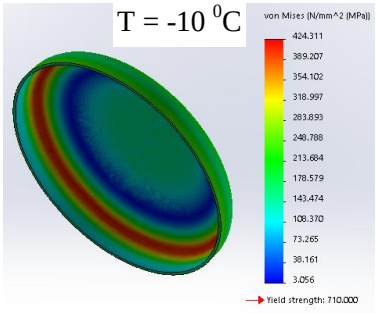

Fig. 23. The Von Mises stress before impact at T = -10 ^{0}C

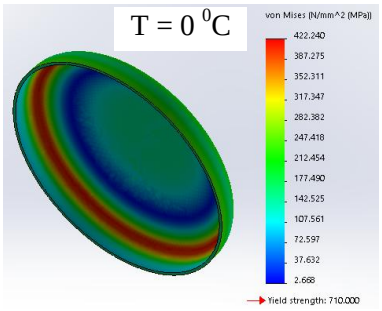

Fig. 24. The Von Mises stress before impact at T = 0 ^{0}C

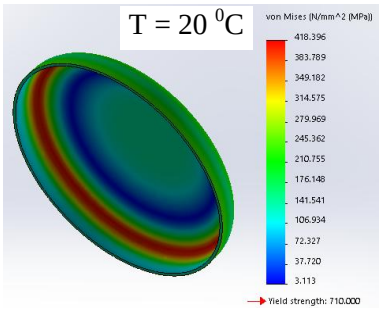

Fig. 25. The Von Mises stress before impact at T = 20 ^{0}C

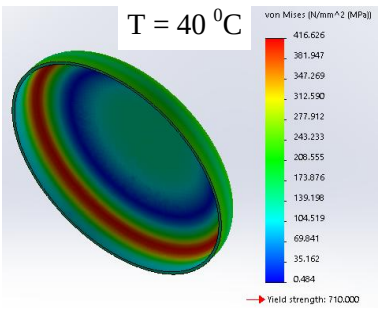

Fig. 26. The Von Mises stress before impact at T = 40 ^{0}C

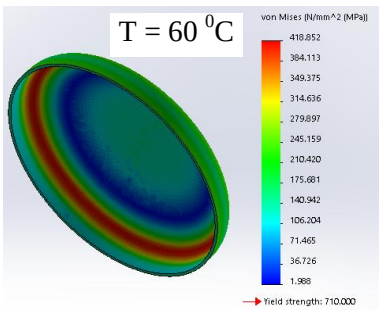

Fig. 27. The Von Mises stress before impact at T = 60 ^{0}C

The numerical summary of influence of the temperature on the stress at the moment of the initial impact (considering that the calculation stress is computed at the temperature T = 0 ^{0}C) is shown in Table 3 and the corresponding variation graph is shown in Figure 28.

Table 3: The Von Mises stress variation given by the influence of temperature in torospheric head cover

T [^{0}C]	-30	-20	-10	0	10	20	30	40	50	60
Δσ [N/mm^2]	6.51	4.24	2.07	0	-1.97	-3.84	-5.4	-5.61	-4.53	-3.39
Δσ [%]	1.52	0.99	0.49	0.00	-0.47	-0.92	-1.30	-1.35	-1.08	-0.81

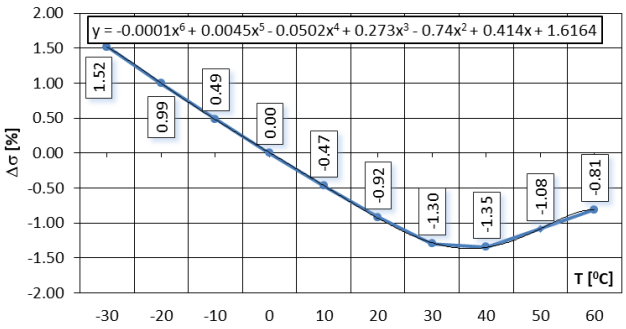

Fig. 28. The procentual deviation of stress given by the temperature at t = 0 μs of impact in head cover

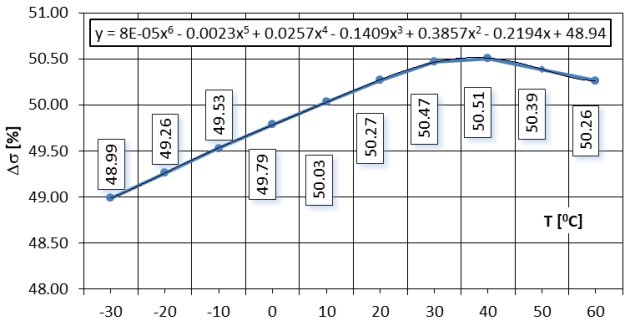

Fig. 29. The procentual variation of Von Mises stress given by impact at t = 40 μs in head cover

The increase in the effort due only to the impact action during the t = 40 μs is shown in Table 4 and the corresponding graph is shown in Figure 29.

Table 4: The Von Mises stress variation given by impact after t = 40 μs in torospheric head cover

T [^{0}C]	-30	-20	-10	0	10	20	30	40	50	60
σ_{impact} [N/mm^2]	210.036	210.094	210.151	204.761	210.263	210.318	210.372	210.425	210.477	210.529
$\sigma_{initial}$ [N/mm^2]	428.75	426.48	424.31	422.24	420.27	418.4	416.84	416.63	417.71	418.85
$\Delta\sigma$ [%]	48.99	49.26	49.53	48.49	50.03	50.27	50.47	50.51	50.39	50.26

The percentage variation in the ratio of the Von Mises stress generated by the temperature and impact is shown in Table 5 and the corresponding graph is given in Figure 30.

Table 5: The procentual variation of Von Mises stress given by ratio of temperature per impact in the torospheric head cover

T [^{0}C]	-30	-20	-10	0	10	20	30	40	50	60
$\Delta\sigma_{initial}$ [N/mm^2]	6.51	4.24	2.07	0.00	-1.97	-3.84	-5.40	-5.61	-4.53	-3.39
$\Delta\sigma_{impact}$ [N/mm^2]	210.036	210.094	210.151	204.761	210.263	210.318	210.372	210.425	210.477	210.529
$\Delta\sigma_{initial}$ / $\Delta\sigma_{impact}$ x 100 [%]	3.10	2.01	0.99	0.00	-0.94	-1.83	-2.57	-2.67	-2.15	-1.61

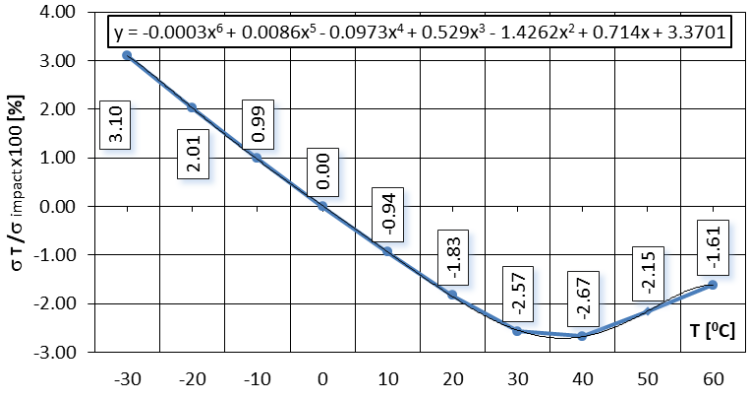

Fig. 30. The graph of Von Mises stress variation ratio $\Delta\sigma_{ini\backslash ial}/\Delta\sigma_{impact}$ x 100 [%] σ(t,T) in torospheric head cover

In the point of contact between the bar and the head cover the state of tension increases sharply in the impact time span of t = 40 μs.
The stress state is graphically shown for: a) t = 40 μs and T = -30 ^{0}C in Figure 31 and Figure 32; b) for T = 60 ^{0}C in Figure 33 and Figure 34.

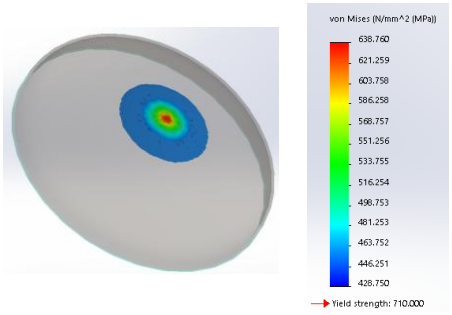

Fig. 31. The Von Mises stress on the superior view of head cover at t = 40 μs and T = - 30 ^{0}C

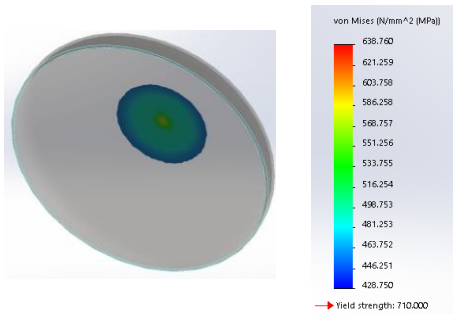

Fig. 32. The Von Mises stress on the inferior view of head cover at t = 40 μs and T = - 30 ^{0}C

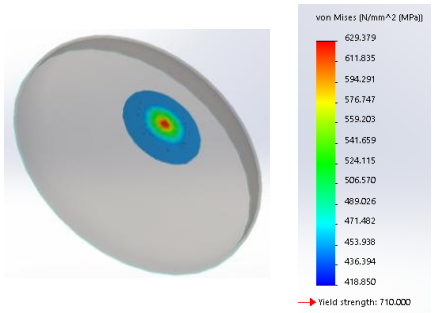

Fig. 33. The Von Mises stress on the superior view of head cover at t = 40 μs and T = 60 ^{0}C

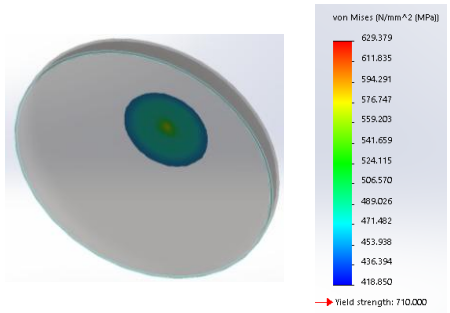

Fig. 34. The Von Mises stress on the inferior view of head cover at t = 40 μs and T = 60 ^{0}C

4. Discussion

From these analyses we can say that:

- for any temperature value, the Von Mises stress increases during impact with the highest value at the negative temperature of T = -30 ^{0}C, as shown in Figures 8 to 17.
- at the beginning of about 20 % of the total impact time there is a moderate increase of the Von Mises stress, after which the highest increase of the effort is made in the next 60 % of the total time, while the remaining 20 % make a small increase until reaching the final value. This is illustrated in the 3D stress-strain graph σ (T, t) from Figure 18.
- the increase of Von Mises stress due to the temperature variation considering that the stress state generated at the temperature T = 0 ^{0}C, (as shown in Table 3), is comprised between the limits $\Delta\sigma_T$ = [-0.81 %...1.52 %] (as shown in Figure 28).
- While the percentage increase in stress due to impact force action is comprised between limits $\Delta\sigma_{impact}$ = [48.49 %...50.51 %], (as shown in Table 4 and Figure 29).
- the ratio between the percentage increase of the stress caused by the temperature and the stress caused by the impact is comprised between limits $\Delta\sigma_T/\Delta\sigma_{impact}$ = [-2.67 %...3.10 %], according the results from Table 5 and Figure 30.
- The front / back views of the cover for the surfaces centered around the impact point show that the effort is higher on the outer contact surface and more attenuated on the inner surface of the cover, as shown in Figures 31 to 34.

5. Conclusions

The following conclusions are drawn from the present study:

a) The highest stresses occurring in the crash test are focused around the point of impact at the contact between the bar and the tank;

b) Increasing effort is done within a very small time interval of order of microseconds;

c) From the onset of impact, there is a short time ≅ 1/5 of the total impact time, which increases slowly, after which they increase very much for ≅ 3/5 of the total impact time, reaching the final effort state;

d) The impact effort overlaps the initial effort of the shell, representing a high percentage of it;
e) The effort made by other causes of stress-generating impact during the impact is very low compared to impact-generated stress;
f) The state of effort is greater on the outer surface around the impact point than the state of effort that occurs on the homologous inner surface around this point;
g) The final conclusion of the simulation results is that the Von Mises stress increase due to impact on the crash test is very important and can not be neglected, representing in this case about 50 % of the Von Mises stress caused by other causes before the impact test.

Financial disclosure: Neither author has a financial or proprietary interest in any material or method mentioned.
Competing interests: The authors declare that they have no significant competing financial, professional or personal interests that might have influenced the performance or presentation of the work described in this manuscript.

References

[1] A.C. Nedelcu, "Romanian automotive industry – analysis made from the intellectual capital perspective", Revista Economica, vol. 67, no. 5, pp. 80-89, 2015;
[2] A. Misztal, N. Belu, N. Rachieru, "Comparative Analysis of Awareness and Knowledge of APQP Requirements in Polish and Romanian Automotive Industry", Applied Mechanics and Materials, vol. 657, pp. 981-985, 2014;
[3] G. Matache, C. Cristescu, u C. Dumitresc, V. Miroiu, "Pregătirea specialiștilor în vederea adaptabilității și creșterii competitivității", Magazine of Hydraulics, Pneumatics, Tribology, Ecology, Sensorics, Mechatronics (HIDRAULICA), no. 3-4, pp. 7-14, 2012. ISSN 1453-7303;
[4] M. Rusănescu, "Material requirements planning, inventory control system in industry", Magazine of Hydraulics, Pneumatics, Tribology, Ecology, Sensorics, Mechatronics (HIDRAULICA), no. 1, pp. 21-25, 2014. ISSN 1453-7303;
[5] Chen Shr-Hung, "Novel design and optimization of vehicle's natural gas fuel tank". Master's Thesis presented to the Faculty of the College of the Engineering and Technology, Ohio University, March 1997;
[6] M.C. Ghiţă, A.C. Micu, M. Ţălu, Ş. Ţălu, E. Adam, "Computer-Aided Design of a classical cylinder gas tank for the automotive industry", Annals of Faculty of Engineering Hunedoara - International Journal of Engineering, Hunedoara, Tome XI, Fascicule 4, pp. 59-64, 2013;
[7] M.C. Ghiţă, A.C. Micu, M. Ţălu, Ş. Ţălu, "Shape optimization of vehicle's methane gas tank", Annals of Faculty of Engineering Hunedoara - International Journal of Engineering, Hunedoara, Tome X, Fascicule 3, pp. 259-266, 2012;
[8] M.C. Ghiţă, A.C. Micu, M. Ţălu, Ş. Ţălu, "3D modelling of a shrink fitted concave ended cylindrical tank for automotive industry". Acta Technica Corviniensis – Bulletin of Engineering, Hunedoara, Romania, Tome VI, Fascicule 4, pp. 87-92, 2013;
[9] M.C. Ghiţă, A.C. Micu, M. Ţălu, Ş. Ţălu, "3D modelling of a gas tank with reversed end up covers for automotive industry", Annals of Faculty of Engineering Hunedoara - International Journal of Engineering, Hunedoara, Tome XI, Fascicule 3, 2013, pp. 195-200, 2013;
[10] M.C. Ghiţă, C.Ş. Ghiță, Ş. Ţălu, S. Rotaru, "Optimal design of cylindrical rings used for the shrinkage of vehicle tanks for compressed natural gas", Annals of Faculty of Engineering Hunedoara - International Journal of Engineering, Hunedoara, Tome XII, Fascicule 3, pp. 243-250, 2014;
[11] M.C. Ghiţă, A.C. Micu, M. Ţălu, Ş. Ţălu, "Shape optimization of a thoroidal methane gas tank for automotive industry", Annals of Faculty of Engineering Hunedoara - International Journal of Engineering, Hunedoara, Tome X, Fascicule 3, pp. 295-297, 2012;
[12] Ş. Ţălu, M. Ţălu, "CAD generating of 3D supershapes in different coordinate systems", Annals of Faculty of Engineering Hunedoara - International Journal of Engineering, Hunedoara, Tome VIII, Fascicule 3, pp. 215-219, 2010;
[13] Ş. Ţălu, M. Ţălu, "A CAD study on generating of 2D supershapes in different coordinate systems", Annals of Faculty of Engineering Hunedoara - International Journal of Engineering, Hunedoara, Tome VIII, Fascicule 3, pp. 201-203, 2010;
[14] C. Bîrleanu, Ş. Ţălu, "Organe de maşini. Proiectare şi reprezentare grafică asistată de calculator" (Machine elements. Designing and computer assisted graphical representations), Cluj-Napoca, Victor Melenti Publishing house, 2001;
[15] Ş. Ţălu, "Limbajul de programare AutoLISP. Teorie şi aplicaţii", (AutoLISP programming language. Theory and applications), Cluj-Napoca, Risoprint Publishing house, 2001;

[16] Ş. Ţălu, "Grafică tehnică asistată de calculator" (Computer assisted technical graphics), Cluj-Napoca, Victor Melenti Publishing house, 2001;
[17] Ş. Ţălu, "Reprezentări grafice asistate de calculator" (Computer assisted graphical representations), Cluj-Napoca, Osama Publishing House, 2001;
[18] Ş. Ţălu, "AutoCAD 2005", Cluj-Napoca, Risoprint Publishing house, 2005;
[19] Ş. Ţălu, M. Ţălu, "AutoCAD 2006. Proiectare tridimensională" (AutoCAD 2006. Three-dimensional designing), Cluj-Napoca, MEGA Publishing house, 2007;
[20] Ş. Ţălu, "AutoCAD 2017", Cluj-Napoca, Napoca Star Publishing house, 2017;
[21] Ş. Ţălu, "Geometrie descriptivă" (Descriptive geometry), Cluj-Napoca, Risoprint Publishing house, 2010;
[22] A. Florescu-Gligore, Ş. Ţălu, D. Noveanu, "Reprezentarea şi vizualizarea formelor geometrice în desenul industrial" (Representation and visualization of geometric shapes in industrial drawing), Cluj-Napoca, U. T. Pres Publishing house, 2006;
[23] A. Florescu-Gligore, M. Orban, Ş. Ţălu, "Cotarea în proiectarea constructivă şi tehnologică" (Dimensioning in technological and constructive engineering graphics), Cluj-Napoca, Lithography of The Technical University of Cluj-Napoca, 1998;
[24] C. Racocea, Ş. Ţălu, "Reprezentarea formelor geometrice tehnice în axonometrie" (The axonometric representation of technical geometric shapes), Cluj-Napoca, Napoca Star Publishing house, 2011;
[25] Ş. Ţălu, C. Racocea, "Reprezentări axonometrice cu aplicaţii în tehnică" (Axonometric representations with applications in technique), Cluj-Napoca, MEGA Publishing house, 2007;
[26] T. Niţulescu, Ş. Ţălu, "Aplicaţii ale geometriei descriptive şi graficii asistate de calculator în desenul industrial" (Applications of descriptive geometry and computer aided design in engineering graphics), Cluj-Napoca, Risoprint Publishing house, 2001;
[27] Ş. Ţălu, "Micro and nanoscale characterization of three dimensional surfaces. Basics and applications", Napoca Star Publishing House, Cluj-Napoca, Romania, 2015;
[28] M. Ţălu, "Calculul pierderilor de presiune distribuite în conducte hidraulice" (Calculation of distributed pressure loss in hydraulic pipelines), Craiova, Universitaria Publishing house, 2016;
[29] M. Ţălu, "Pierderi de presiune hidraulică în conducte tehnice cu secţiune inelară. Calcul numeric şi analiză C.F.D." (Hydraulic pressure loss in technical piping with annular section. Numerical calculation and C.F.D.), Craiova, Universitaria Publishing house, 2016;
[30] M. Ţălu, "Mecanica fluidelor. Curgeri laminare monodimensionale" (Fluid mechanics. The monodimensional laminar flow), Craiova, Universitaria Publishing house, 2016;
[31] M. Ţălu, "The influence of the corrosion and temperature on the Von Mises stress in the lateral cover of a pressurized fuel tank", Magazine of Hydraulics, Pneumatics, Tribology, Ecology, Sensorics, Mechatronics (HIDRAULICA), no. 4, pp. 89-97, 2017, ISSN 1453-7303;
[32] Ş. Ţălu, M. Ţălu, "The influence of deviation from circularity on the stress of a pressurized fuel cylindrical tank", Magazine of Hydraulics, Pneumatics, Tribology, Ecology, Sensorics, Mechatronics (HIDRAULICA), no. 4, pp. 34-45, 2017, ISSN 1453-7303;
[33] M. Bică, M. Ţălu, Ş. Ţălu, "Optimal shapes of the cylindrical pressurized fuel tanks", Magazine of Hydraulics, Pneumatics, Tribology, Ecology, Sensorics, Mechatronics (HIDRAULICA), no. 4, pp. 6-17, 2017, ISSN 1453-7303;
[34] T. Ambati, K.V.N.S. Srikanth, P. Veeraraju, "Simulation of vehicular frontal crash-test", International Journal of Applied Research in Mechanical Engineering (IJARME), vol. 2, issue 1, pp. 37-42, 2012.
[35] W. Pawlus, H.R. Karimi, K.G. Robbersmyr, "Mathematical modeling of a vehicle crash test based on elasto-plastic unloading scenarios of spring–mass models", The International Journal of Advanced Manufacturing Technology, vol. 55, pp. 369–378, 2011;
[36] W. Pawlus, H.R. Karimi, K.G. Robbersmyr, "Investigation of vehicle crash modeling techniques: theory and application", The International Journal of Advanced Manufacturing Technology, vol. 70, issue 5–8, pp. 965–993, 2014;
[37] G. Šušteršić, I. Grabec, I. Prebil, "Statistical model of a vehicle-to-barrier collision", International Journal of Impact Engineering, vol. 34, Issue 10, pp. 1585-1593, 2007;
[38] K. Haleem, P. Alluri, A. Gan, "Investigating fractal characteristics in crash trends for potential traffic safety prediction", Proceedings of the 95th Annual Meeting of the Transportation Research Board, Washington DC, United States, 2016;
[39] Yu Rende, Shen Juan, "Analysis on road traffic accidents spatial distribution based on the multi-fractal theory", Computer Modelling & New Technologies, vol. 18, no. 7, pp. 283-289, 2014;
[40] Chen Peng, Li Xu-hong, Sun Hua-can, "Analysis of Traffic Accident Based on Fractal Theory", Journal of Highway and Transportation Research and Development, vol. 25, no. 3, pp. 130-3, 2008;
[41] Zhang Xiao-hong, Yu Ren-de, Zhang Qiang, "Traffic accidents analysis based on multi-fractal spectrum", Journal of Shandong University of Technology (Natural Science Edition), vol. 27, no. 2, pp. 62-64, 2013;
[42] *** Autodesk AutoCAD 2017 software;
[43] *** SolidWorks 2017 software.